Wind and Structures, *Vol. 30, No. 4 (2020) 393-403*
DOI: https://doi.org/10.12989/was.2020.30.4.393

Nonlinear Kalman filter bias correction for wind ramp event forecasts at wind turbine height

Jing-Jing Xu[1a], Zi-Niu Xiao[*2] and Zhao-Hui Lin[1]

[1]*International Center for Climate and Environment Science (ICCES), Institute of Atmospheric Physics, Chinese Academy of Science, Beijing 100029, China*
[2]*State Key Laboratory of Numerical Modeling for Atmospheric Sciences and Geophysical Fluid Dynamics (LASG), Institute of Atmospheric Physics, Chinese Academy of Sciences, Beijing 100029, China*

(Received June 17, 2019, Revised March 20, 2020, Accepted March 28, 2020)

Abstract. One of the growing concerns of the wind energy production is wind ramp events. To improve the wind ramp event forecasts, the nonlinear Kalman filter bias correction method was applied to 24-h wind speed forecasts issued from the WRF model at 70-m height in Zhangbei wind farm, Hebei Province, China for a two-year period. The Kalman filter shows the remarkable ability of improving forecast skill for real-time wind speed forecasts by decreasing RMSE by 32% from 3.26 m s_{-1} to 2.21 m s_{-1}, reducing BIAS almost to zero, and improving correlation from 0.58 to 0.82. The bias correction improves the forecast skill especially in wind speed intervals sensitive to wind power prediction. The fact shows that the Kalman filter is especially suitable for wind power prediction. Moreover, the bias correction method performs well under abrupt weather transition. As to the overall performance for improving the forecast skill of ramp events, the Kalman filter shows noticeable improvements based on POD and TSS. The bias correction increases the POD score of up-ramps from 0.27 to 0.39 and from 0.26 to 0.38 for down-ramps. After bias correction, the TSS score is significantly promoted from 0.12 to 0.26 for up-ramps and from 0.13 to 0.25 for down-ramps.

Keywords: numerical simulation; wind power prediction; bias correction; nonlinear Kalman filter; WRF model

1. Introduction

Wind energy production has undergone rapid growth in China recently (Chen and Tran 2015). Due to variability and uncertainty of wind field in atmospheric boundary layer, wind energy, unlike traditional resources, varies substantially over both time and space (Lange and Focken 2006). Therefore, we need accurate forecasts to optimize wind power generation (Costa *et al*. 2008, Burton *et al*. 2001, Cheng *et al*. 2015, Deppe *et al*. 2013, Dhunny *et al*. 2015).

One of the growing concerns for wind energy production is wind ramp events (Gunter *et al*. 2017, Yang *et al*. 2013), which are rapid changes in wind power output due to abrupt changes in wind speed (Freedman *et al*. 2008). Wind ramp events can be costly for both wind farms and grid operators, and consequently, the ability to forecast ramp events is becoming a crucial issue (Francis 2008. Bradford *et al*. 2010). Researchers found that large ramp events which cause 50% or greater change of the wind power capacity occurred less than 7% of the time within 4 hours (Greaves *et al*. 2009) and occurred less than 4% of the time within 2 hours (Zack 2007). So ramp events are difficult to forecast because of their rareness.

[*]Corresponding author, Professor
E-mail: xiaozn@lasg.iap.ac.cn
[a]Ph. D.
E-mail: xujingjing@mail.iap.ac.cn

For years, there have been few studies of wind forecasts at turbine height (about 60 - 100 m). Researchers traditionally focused on wind forecasts at 10-m height (Delle Monache *et al*. 2011, Crochet 2004, Muller 2011, Zhang *et al*. 2013), at which official wind observations are taken. For wind ramp event forecasts, even fewer studies were addressed before (Bradford *et al*. 2010, Deppe *et al*. 2013).

Studies have demonstrated that numerical weather prediction models can have significant systematic and random errors for wind speed predictions (Jordan 2007, Yim *et al*. 2007, Deppe *et al*. 2013, Rife and Davis 2005, Hu *et al*. 2013). One approach to obtain more accurate prediction is to use the post-processing bias correction approaches based on statistical methods (Glahn and Lowry 1972, Stensrud and Yussouf 2003, Hacker and Rife 2007, Xu *et al*. 2013, Xu *et al*. 2014). One of the most successful methods is Kalman filter (Kalman 1960, Kalman and Bucy 1961, Kalnay 2002). The Kalman filter is the statistically optimal sequential estimation procedure in which observations are recursively combined with recent forecasts in order to minimize the corresponding biases, and it needs minor computational costs and can easily adapt to any alteration of the observation. During the last several years, the Kalman filter has been used for improving weather forecasts by successfully reducing the bias of forecasting continuous variables such as 2 m temperature, 10 m wind speed and ozone concentration (Homleid 1995, Crochet 2004, Muller 2011, Delle Monache *et al*. 2006, Delle Monache *et al*. 2008, McCollor and Stull 2008, Rincon *et*

http://www.techno-press.com/journals/was&subpage=7
ISSN: 1226-6116 (Print), 1598-6225 (Online)

al. 2010), mostly focusing on diurnal bias.

The structure of Kalman filter algorithms of the above type is more suitable to describe linear procedures. And consequently, the application on variables following nonlinear or discontinuous behaviors is always questionable. Wind ramp events have rapid variations, which mean high non-linearity. Therefore, while the application of Kalman filters for improving air temperature forecasts seems to be successful in many cases, analogous work for wind speed forecasts, especially for real-time wind speed forecasts, may lead to poor results (Giebel 2001). However, the application of nonlinear functions for classical Kalman filter makes it possible for simulating nonlinear procedures. Galanis *et al*. (2006) proposed nonlinear polynomial mappings of the Kalman filter to better simulate nonlinear problems in numerical weather prediction, and the method was successfully applied to 24 h-72 h wind speed forecasts of 1-h temporal resolution at turbine height (Louka *et al*. 2008).

However, wind speed forecasts of 15-min temporal resolution, which were not referred to in the previous work (Louka *et al*. 2008), are needed for wind power prediction. Moreover, there're two kinds of wind speed forecasts for wind power prediction according to the demands of wind energy industry: short-term forecasts with forecast period of 24 h-72 h, and real-time forecasts with period of 15 min-4 h. Traditionally, the real-time wind speed forecasts are acquired by statistical methods, but we attempt to apply numerical model and the bias correction to improve the forecast skill. Is the Kalman filter based on polynomial function suitable for real-time wind speed forecasts? How effectively can the nonlinear Kalman filter improve the wind ramp event forecasts? These are the main purposes of our work.

In this paper, firstly, we provide the implementation of a nonlinear polynomial Kalman filter bias correction method. Section 3 outlines the model configuration and the design of the experiment, and section 4 describes the verification statistics for evaluating the bias correction performance. Thereafter, in section 5 a detailed study of nonlinear Kalman filter application to wind speed at turbine height obtained at Zhangbei wind farm for two years, is illustrated. In this section, we mainly focused on evaluating the effectiveness of the optimal filter for improving wind ramp event forecasts. Finally, the paper closes with a summary and conclusions in section 6.

2. Methodology

2.1. The nonlinear Kalman filter bias correction method

The basic concept of the general Kalman filter theory was presented in Kalman (1960), Kalman and Bucy (1961), and Kalnay (2002). In our study, we slightly modified the nonlinear Kalman filter proposed by Galanis *et al*. (2006) and the procedure is introduced as follows. First, we focused on a special meteorological variable (wind speed at turbine height) in time, based on estimating the forecast bias

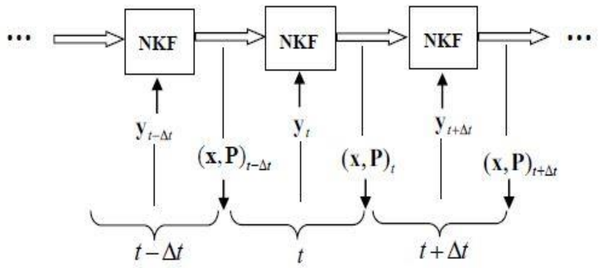

Fig. 1 Schematic diagram of the NKF (nonlinear Kalman filter) procedure

of wind speed as a function of the previous forecast bias rather than the direct model output in Galanis *et al*. (2006). Specifically, if we denote the forecast bias of the numerical model at time t by y_t and the previous forecast bias by y_{t-1}, then the current forecast bias y_t can be composed as a polynomial of y_{t-1}

$$y_t = x_{0,t} + x_{1,t}\cdot y_{t-1} + x_{2,t}\cdot y_{t-1}{}^2 + \ldots + x_{n-1,t}\cdot y_{t-1}{}^{n-1} + v_t \tag{1}$$

where the coefficients ($x_{i,t}$) are the parameters estimated by the filter and v_t is the Gaussian non-systematic error. Therefore, the state vector is formed by the coefficients ($x_{i,t}$): $\mathbf{x}_t = [x_{0,t}, x_{1,t}, x_{2,t}, \ldots, x_{n-1,t}]^T$. On the other hand, the observation matrix takes the form $\mathbf{H}_t = [1, y_{t-1}, y_{t-1}{}^2, \ldots, y_{t-1}{}^{n-1}]$. Hence the system equation and the observation equation correspondingly take the form respectively

$$\mathbf{x}_t = \mathbf{x}_{t-\Delta t} + \mathbf{w}_t\,, \qquad \mathbf{y}_t = \mathbf{H}_t\mathbf{x}_t + \mathbf{v}_t \tag{2}$$

The random vectors $\mathbf{w}_t$ and $\mathbf{v}_t$ have to follow the normal distribution with zero mean and must be independent. The time delay Δt denotes the time period of previous step when we can use the information of true values, so the time delay implies the forecast period. It is 1 h, 2 h, 4 h respectively in this paper.

Kalman filter theory (Kalman 1960) gives a method recursively estimating the unknown state vector $\mathbf{x}_t$ until all the values y up to time t. The optimal estimate that we can give for the state vector $\mathbf{x}_t$ and the covariance matrix $\mathbf{P}_t$ at time t are

$$\mathbf{x}_{t/t-\Delta t} = \mathbf{x}_{t-\Delta t}\,, \qquad \mathbf{P}_{t/t-\Delta t} = \mathbf{P}_{t-\Delta t} + \mathbf{W}_t \tag{3}$$

As soon as the new value $\mathbf{y}_t$ becomes known, we calculate the new value of state vector $\mathbf{x}_t$

$$\mathbf{x}_t = \mathbf{x}_{t/t-\Delta t} + \mathbf{K}_t(\mathbf{y}_t - \mathbf{H}_t\mathbf{x}_{t/t-\Delta t}) \tag{4}$$

where

$$\mathbf{K}_t = \mathbf{P}_{t/t-\Delta t}\mathbf{H}_t{}^T(\mathbf{H}_t\mathbf{P}_{t/t-\Delta t}\mathbf{H}_t{}^T + \mathbf{V}_t)^{-1} \tag{5}$$

is the most crucial parameter of the filter, the Kalman gain matrix. It determines how easily the filter will adjust to any possible new conditions. Finally, the new value of the covariance matrix $\mathbf{P}_t$ of the unknown state is given by

$$\mathbf{P}_t = (\mathbf{I} - \mathbf{K}_t \mathbf{H}_t)\mathbf{P}_{t/t-\Delta t} \tag{6}$$

Eqs. (3) - (6) are known as updating equations, which update the Kalman algorithm from time $t-\Delta t$ to t. Note that T, -1 denotes the transpose matrix and the inverse matrix respectively, while **I** stands for the identity matrix. The schematic diagram of the procedure is shown in Fig. 1.

The initial values $\mathbf{x}_0$, $\mathbf{P}_0$ must be defined before running the filter, but they do not affect the results seriously, since $\mathbf{x}_t$ and $\mathbf{P}_t$ will converge to their true values very soon. However, things are different with the covariant matrixes $\mathbf{W}_t$ of the random vector $\mathbf{w}_t$ and $\mathbf{V}_t$ of $\mathbf{v}_t$. The way that they are calculated during the process affects the Kalman gain and thus crucially affects the final outcome. Many authors (Homleid 1995, Delle Monache 2006) consider them to be time independent, thereby losing the capability of making quicker adjustments to possible external changes. In our case, we estimate the system covariance matrix $\mathbf{W}_t$ and the observation covariance matrix $\mathbf{V}_t$ based on the sample of the last 7 values of $\mathbf{w}_t = \mathbf{x}_t - \mathbf{x}_{t-1}$ and $\mathbf{v}_t = \mathbf{y}_t - \mathrm{H}_t\mathbf{x}_t$ respectively

$$\mathbf{W}_t = \frac{1}{n-1}\sum_{i=1}^{n}((\mathbf{x}_{t-i} - \mathbf{x}_{t-i-1}) - \frac{\sum_{j=1}^{n}(\mathbf{x}_{t-j} - \mathbf{x}_{t-j-1})}{n})^2 \tag{7}$$

$$\mathbf{V}_t = \frac{1}{n-1}\sum_{i=1}^{n}((\mathbf{y}_{t-i} - \mathbf{H}_{t-i}\mathbf{x}_{t-i}) - \frac{\sum_{j=1}^{n}(\mathbf{y}_{t-j} - \mathbf{H}_{t-j}\mathbf{x}_{t-j})}{n})^2 \tag{8}$$

where n = 7 and n-1 represents unbiased estimation. The time period of 7 values has proved to be the optimal choice in our study for successful correction and fast adaptability, and can be changed for other cases. Here we assume the initial value $\mathbf{x}_0$ of the state vector to be 0, and the initial covariance matrix $\mathbf{P}_0$ to be diagonal with the diagonal elements having a considerably large value (here we propose 4), which indicates that we do not really trust our first guess. Above Eqs. (1) - (8) show the procedure of our nonlinear Kalman filter algorithm.

2.2. Definition of ramp events

We define a ramp event to exist when the change in wind power is 50% or more of capacity over a time interval of 4 hours or less (Greaves *et al*. 2009). The changes for wind power can be transformed to the changes for wind speed according to the wind turbine power curve (Fig. 2). From Fig. 2, we can see that when the wind is equal to or less than 5 m s^{-1} (the cut-in speed) a turbine will not generate power output, while once the speed exceeds 12 m s^{-1} (the rated wind speed), the wind turbine begins to perform at maximum capability (100% capacity). On the other hand, when wind speed approaches 25 m s^{-1}, the power output will plummet to 0 caused by the high-speed shutdown of turbines. The power curve of wind turbine suggests that ramp events occurring between the cut-in speed and the rated wind speed are extremely costly for wind energy production because they may cause blackouts and overload the grid (Francis 2008, Deppe *et al*. 2013). Hence increase or decrease of more than 3.5 m s^{-1} within 4 hours or less for wind speeds within 5-12 m s^{-1} is considered to be a ramp event.

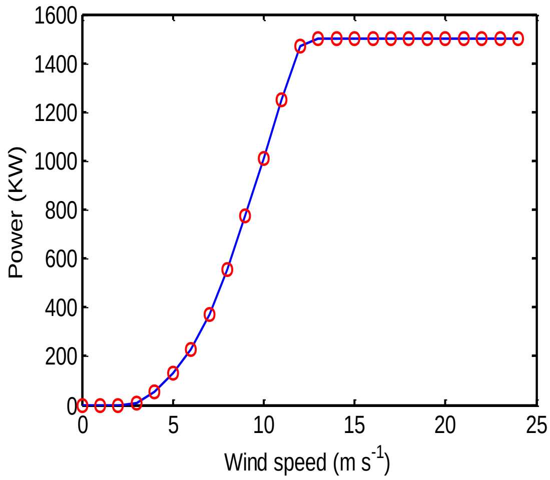

Fig. 2 Power curve for the 1.5-MW wind turbines used at the Zhangbei wind farm. Cut-in speed is around 5 m s^{-1} while the rated wind speed is around 12 m s^{-1}

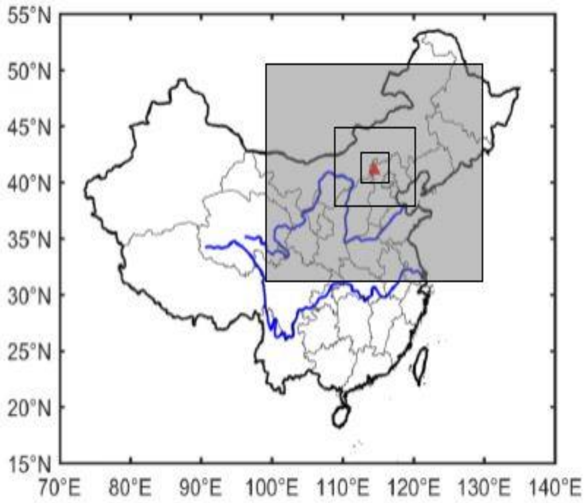

Fig. 3 Zhangbei wind farm is located in Hebei Province, China. The red solid triangle denotes the observation station and the gray shades denote the three nested domains

3. Model and experiment description

Zhangbebi wind farm is located northwest of Hebei Province, China (see Fig. 3). The farm consists of 66 wind turbines each with capacity of 1.5MW, and the total installed capacity of wind power is about 100MW. The wind turbine height is 70 m, and the area of the wind farm is approximately 35 km^2 which covers complex mountain terrain with the altitude ranging from about 1600 to 1800 m.

The bias correction method described in section 2 is applied to 24-h wind speed forecasts (at 10-min increments) issued from the WRF model (Skamarock *et al*. 2008). Observation data for this study was obtained from one mast sited at Zhangbei wind farm for two years from 1 January

2016 to 31 December 2017 (totally 731 days), with the latitude 41°03'N, the longitude 114°29'E and the altitude 1660 m. The average wind speed and direction were recorded for every 10-min interval by NRG anemometer.

The WRF model is run over the northeastern China with 3 nested domains centered on Zhangbei wind farm using two-way nesting, having 27-km, 9-km, and 3-km horizontal grid increments respectively (each domain have 98*76 grids) (see Fig. 3) and 37 vertical levels (12 levels are located in the lowest 1 km with sigma values: 1, 0.998, 0.996, 0.994, 0.992, 0.989, 0.983, 0.97, 0.954, 0.934, 0.909, 0.88). Initial and boundary conditions were obtained from the GFS/NCEP data at a resolution of 0.5 degree. The model is initialized at 1800 UTC each day and run for 30 hours. The first 6 hours are removed as model spin-up, and we use the remaining 24 h outputs. The 70-m wind speed forecasts within the finest domain, obtained by vertical interpolation, were bilinearly interpolated to the observation location.

The parameterization schemes for the experiment are as follows: the Mellor-Yamada-Janjic scheme (Mellor and Yamada 1982) for the planetary boundary layer, the Noah land surface model (Chen and Dudhia 2001) for the land surface scheme, the Eta scheme (Janjic 1994) for the surface layer, the Purdue Lin microphysics scheme (Lin *et al*. 1983), the Kain-Fritsch scheme (Kain 2004) for the convective parameterization (only in the two coarser domains), the Rapid Radiation Transfer Model (RRTM) scheme (Mlawer *et al*. 1997) and the Goddard scheme (Chou and Suarez 1994) for the longwave and shortwave radiation schemes respectively.

The planetary boundary layer (PBL) turbulence is especially influential in the simulation of low level atmospheric winds and diffusion of dynamical and thermodynamical quantities. The MYJ PBL scheme uses the 1.5-order turbulence closure of Mellor and Yamada (1982) to represent turbulence above the surface layer (Janjic 1994). The MYJ scheme determines eddy diffusion coefficients from prognostically calculated turbulent kinetic energy (TKE). The simulation of many processes in boundary layer such as thermally induced circulations (mountain-valley and sea breezes) and terrain-forced flow, of which are characterized properly in the MYJ PBL scheme, is very important for the prediction of local wind in complex terrain. Low-level jets, which can increase wind speeds at turbine heights and also can create large stress on the turbines causing fatigue issues, have noticeable influences on the wind power industry. Mellor and Yamada (1982) argue that the MYJ scheme is appropriate for all stable and slightly unstable flows because of the local closure with the assumption of small scale eddy. Because the observed low-level jets typically occur at night under stable conditions, the MYJ scheme is particularly suitable for simulation of low-level jets.

When performing the nonlinear Kalman filter bias correction, we first transform the observations and forecasts to one-hour averages. Then remove the results for the first day (24 time steps when Δt = 1h, 12 time steps when Δt = 2h, 6 time steps when Δt = 4h correspondingly) to eliminate the effects of filter algorithm's spin-up, and then analyze the results for the remaining 730 days. Finally, we transform the one-hour wind speeds back to 10-min wind speeds.

4. Verification statistics

We applied the following metrics to evaluate the performance of the bias correction method

$$BIAS = \frac{1}{N_p}\sum_{i=1}^{N_p}(F_i - O_i) \tag{9}$$

where *BIAS* denotes the mean error, O_i is the observation value at time i, and F_i is the corresponding forecast value. N_p is the size of sample which means the number of pairs (F_i, O_i). Note that the subscripts p denotes prediction.

$$MAE = \frac{1}{N_p}\sum_{i=1}^{N_p}\left|F_i - O_i\right| \tag{10}$$

where *MAE* denotes the mean absolute error.

$$RMSE = \sqrt{\frac{1}{N_p}\sum_{i=1}^{N_p}(F_i - O_i)^2} \tag{11}$$

where *RMSE* denotes the root mean square error.

$$r = \frac{\sum_{i=1}^{N_p}(F_i - \bar{F})(O_i - \bar{O})}{\sqrt{\sum_{i=1}^{N_p}(F_i - \bar{F})^2 \sum_{i=1}^{N_p}(O_i - \bar{O})^2}} \tag{12}$$

where r denotes Pearson correlation coefficient, $\bar{F}$ and $\bar{O}$ is the mean forecast value and observation value respectively.

For evaluating ramp events, a contingency table was used for evaluating accuracy (see Table 1). Our metrics include the probability of detection (*POD*), the false-alarm ratio (*FAR*), the threat score (*TS*), and the true skill score (*TSS*). These quantities are given as Eqs. (13) - (16).

$$POD = \frac{A}{A+C} \tag{13}$$

$$FAR = \frac{B}{A+B} \tag{14}$$

$$TS = \frac{A}{A+B+C} \tag{15}$$

$$TSS = \frac{AD - BC}{(A+C)(B+D)} \tag{16}$$

5. Results

5.1. Sensitivity analysis

The method presented in section 2 outlines the procedure for applying nonlinear functions for reducing the

Table 1 Contingency table definition, where A to D is the counts of events in each category, out of N total events

		Observation	
		Yes	No
Forecast	Yes	*A*	*B*
	No	*C*	*D*

Table 2 The overall performance of the Kalman filter based on four metrics (BIAS, MAE, RMSE, correlation coefficient) using polynomials of zero to third order against the model direct output

Statistics	Raw	0-order	1-order	2-order	3-order
BIAS (m s^{-1})	0.31	0.13	0.09	0.03	0.04
MAE (m s^{-1})	2.52	1.98	1.79	1.66	1.67
RMSE (m s^{-1})	3.26	2.71	2.42	2.21	2.22
Correlation coefficient	0.58	0.72	0.78	0.82	0.82

Table 3 The overall performance of the Kalman filter based on four metrics (BIAS, MAE, RMSE, correlation coefficient) with different time delay Δt against the model direct output

Statistics	Raw	One hour	Two hours	Four hours
BIAS (m s^{-1})	0.31	0.03	0.08	0.29
MAE (m s^{-1})	2.52	1.66	2.09	2.52
RMSE (m s^{-1})	3.26	2.21	2.74	3.32
Correlation coefficient	0.58	0.82	0.73	0.61

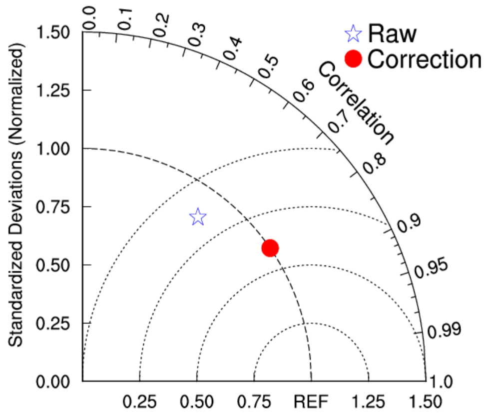

Fig. 4 Taylor diagram showing the raw forecasts and the bias correction

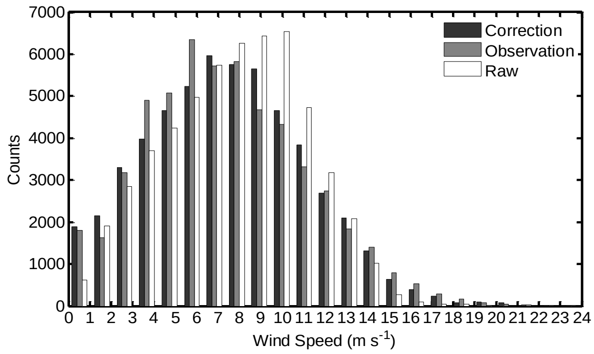

Fig. 5 Counts of the binned wind speed of the observation, the raw forecasts and the bias correction

forecast error in real-time wind speed forecasts. In this subsection, polynomials of different orders are applied to obtain the optimal order based on the best performance of the filter in improving the wind speed forecasts. As to different time delay Δt, theoretically, the shorter the time delay is, the higher the forecast accuracy is, because we can use the information of recent observation data. However, longer time delay means extending the forecast period. So we also need to examine the sensitivity of the filter with the time delay Δt besides the polynomial order.

First we fix the time delay Δt = 1h to investigate to which extent the increase of the polynomial order influences the performance of the filter. Table 2 presents the overall performance of the Kalman filter based on four metrics (BIAS, MAE, RMSE, correlation coefficient) using polynomials of zero to third order upon the direct model output. The results imply that when the order of the Kalman filter gets higher, the improvement of forecasts increases. But when the order exceeds two, the improvement becomes stable. So the order of two is the optimal choice. For all cases BIAS is nearly eliminated to zero indicating that the main goal of the Kalman filter is achieved. The significant reduction of MAE and RMSE for the Kalman filter of the second order confirms that the discrepancy between the observations and forecasts has been reduced regardless of any type of the errors. The attempt to use higher order polynomials does not lead to additional improvements of the filter. On the contrary, much instability arises in predicting the wind speed series, and thus the performance of the filter deviates from the optimal value.

Table 3 gives the overall performance of the Kalman filter based on four metrics (BIAS, MAE, RMSE, correlation coefficient) with different time delay Δt against the model direct output. It is not surprising that the filter with one-hour time delay shows the best performance, and when the time delay gets longer, the correction accuracy becomes worse. The algorithm with two-hour time delay also shows fine correction efficiency, while the filter with four-hour time delay does not show positive influence at all.

In the present study, we choose the results with the second-order polynomial and one-hour time delay to assess the global performance and especially the performance for ramp event forecasts.

5.2. Global performance and diurnal trend climatology

In this subsection the global performance of the Kalman filter bias correction is evaluated with the direct model output. First we use the Taylor diagram (Fig. 4) to display the extent of the pattern correspondence between prediction and observation. In the Taylor diagram the radial distance from the origin is the normalized standard deviation (NSD) for prediction, the azimuthal position denotes the correlation coefficient, and then the distance to the point

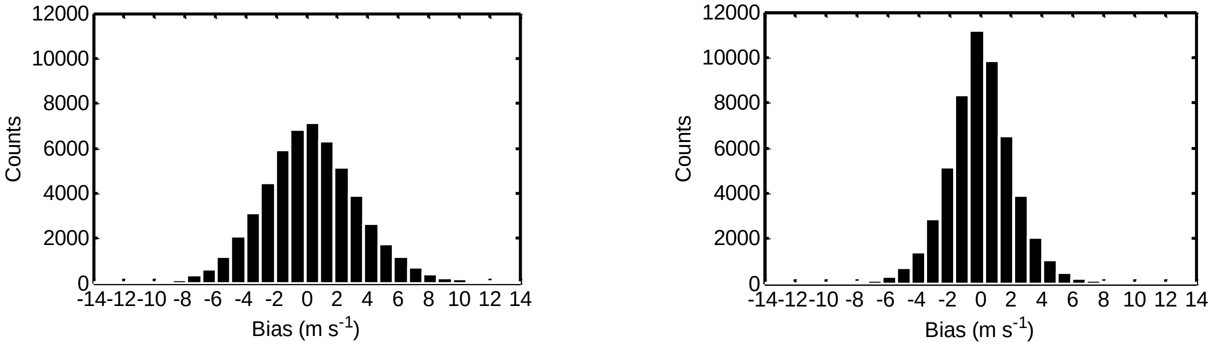

(a) Raw forecasts (b) Bias correction

Fig. 6 Bias distribution of the raw forecasts and the bias correction

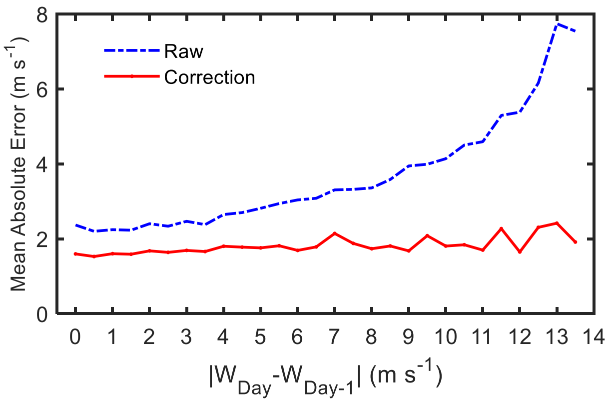

(a) The forecast absolute error of the raw forecasts and the bias correction as a function of the day-to-day wind speed variation

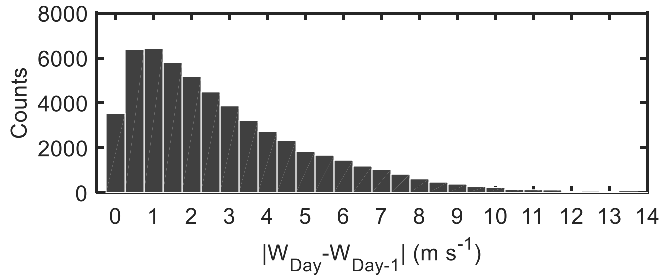

(b) Counts of the binned magnitude of the day-to-day variation of wind speed

Fig. 7

representing the observation (REF) is proportional to the central root mean square error (CRMSE) of the prediction. From Fig. 4 we can see that the correction is much closer to the observation compared with the raw forecasts. The correction has a better NSD, close to the perfect value of 1, which means the standard deviation of the forecasts is equal to the standard deviation of the observation, while the raw forecasts underestimate the standard deviation. Meanwhile, the Kalman filter method improves the pattern correlation with observation when compared to the raw forecasts, moving closer to the REF point with lower CRMSE.

Table 3 characterizes the ability of improving forecast skill for the bias correction quantitatively. The Kalman filter has decreased RMSE by 32% from 3.26 m s^{-1} to 2.21 m s^{-1}, decreased MAE by 34% from 2.52 m s^{-1} to 1.66 m s^{-1}, reduced BIAS almost to zero, and improved the correlation from 0.58 to 0.82. All the metrics show remarkable improvements. Fig. 5 gives the wind speed distribution of the observation, the raw forecasts and the correction. The bias correction improves the forecast skill in almost all wind speed intervals. In wind speed intervals 8-12 m s^{-1}, included in the area sensitive to wind power prediction, the correction shows prominent efficiency. The results show that the Kalman filter is especially suitable for wind power prediction. In Fig. 6 the bias distribution for the raw forecasts and the bias correction is presented. The histograms show clearly that the bias-corrected wind speeds lead to a sharper distribution of the bias meaning much closer to zero, and the distribution is more symmetrical than for the raw forecasts. Consequently, the forecasts after bias correction present lower uncertainty.

Under weather transitions such as front passage,

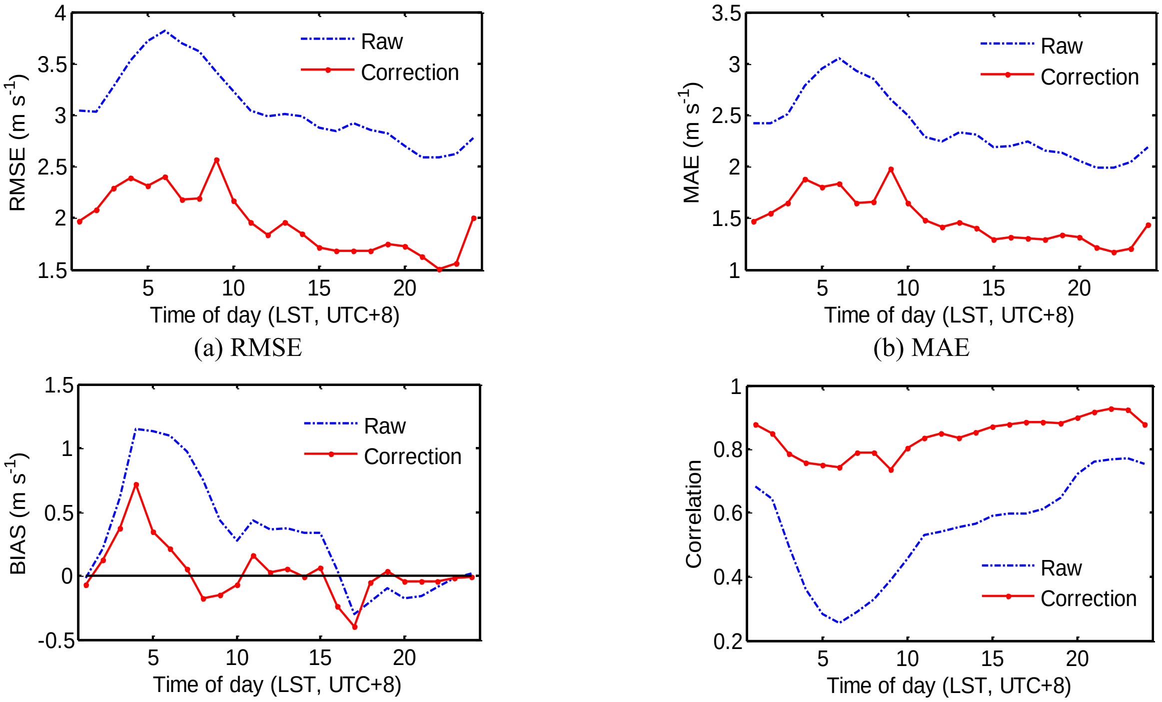

(a) RMSE (b) MAE

(c) BIAS (d) Correlation

Fig. 8 Temporal evolution of the metrics for the raw forecasts and the bias correction across the 24h of forecast. The time of day is the local standard time (LST)

thunderstorm, the changes of wind speeds can be very large. In order to evaluate the performance of the bias correction method under abrupt weather transition, we investigate the forecast skill of the raw forecasts and the bias correction as a function of the day-to-day variation of wind speed ($|W_{day}$ - $W_{day-1}|$) (see Fig. 7(a)). W_{day-1} denotes the wind speed of previous day, which means that before 24 hours. Fig. 7(b) shows that the day-to-day variation, binned in increments of 0.5 m s^{-1}, is mainly distributed in 0-6 m s^{-1}, and the probability of $|W_{day}$ - $W_{day-1}|$ gets smaller as it grows. The forecast error starts at 2.4 m s^{-1} and 1.6 m s^{-1} for the raw forecasts and the bias correction respectively. And the forecast error for the raw forecasts keeps about 0.8 m s^{-1} larger than that for the bias correction until $|W_{day}$ - $W_{day-1}|$ bigger than 4 m s^{-1}, and ascends rapidly achieving 4.1 m s^{-1} when $|W_{day}$ - $W_{day-1}|$ is equal to 10 m s^{-1}; while that for the bias correction varies with small amplitude between 1.5-2.1 m s^{-1}. The results for $|W_{day}$ - $W_{day-1}|$ bigger than 10 m s^{-1} do not have statistical meaning because of too few samples. The above results suggest that when the day-to-day variation is large, the bias correction improve the forecast skill effectively, and the nonlinear Kalman filter performs well under weather transition.

To investigate the diurnal characteristics of the forecast errors, we compute the four metrics with all the available data at a given time, which is each of the 24 forecast hours. Fig. 8 shows the temporal evolution of RMSE, MAE, BIAS, and correlation, respectively.

The growth of the planetary boundary layer (PBL) is often a challenging process to be predicted (Deppe *et al.* 2013), which is reflected by the jump in RMSE value before sunrise (04 LST-08 LST) (Fig. 8(a)). Throughout the daytime and early evening, the RMSE value stays constant around 3 m s^{-1}. Around sunrise, the raw forecasts show an increase in RMSE, given the uncertainty associated with the PBL growth. Based on RMSE, the Kalman filter shows improvement across all the forecast hours in the range about 1 m s^{-1} with respect to the raw, while decreasing RMSE around 1.5 m s^{-1} in 05 LST-08 LST. This is the indication of the Kalman filter method's ability to improve the predictive skill. As for MAE (see Fig. 8(b)), the temporal variation is similar to RMSE. While for the correlation coefficient (Fig. 8(d)), the Kalman filter method significantly improves the correlation for all the 24 forecast hours, especially for 04 LST-08 LST providing average improvements of correlation around 0.5 with respect to the raw forecasts.

For BIAS (Fig. 8(c)), the raw forecasts also exhibit a strong diurnal cycle with a peak before sunrise when the growth of the PBL is occurring, and almost zero throughout the daytime and early evening. The Kalman filter method drastically reduces the bias of the raw forecasts having values close to zero at most time of the day, and nearly reduces it by around 0.8 m s^{-1} constant-in-time in 05 LST-07 LST.

5.3. Evaluation of ramp event forecasts

In this subsection, we focus on the accuracy of ramp event forecasts at turbine height. A contingency table (see Table 1) is applied to classify the forecasted and observed ramp events into hits, false alarms, misses, and correct nulls. A ramp event is considered to be a hit if it occurred 4 h before or after the forecast time, that is, if a ramp is forecasted at time *T*, then we consider the forecast a hit if

Table 4 Number of ramp events for each ramp type. POD, FAR, TS, and TSS scores are calculated for the raw forecasts and the bias correction

Ramp type	Statistics	Raw	Correction	Obs. total events	Model total events	Correction total events
Up-ramp	POD	0.27	0.39	360	390	404
	FAR	0.75	0.65			
	TS	0.15	0.23			
	TSS	0.12	0.26			
	Correct Null	1628	1658			
Down-ramp	POD	0.26	0.38	363	349	385
	FAR	0.73	0.64			
	TS	0.15	0.23			
	TSS	0.13	0.25			
	Correct Null	1662	1671			

there is an observed ramp on the time interval [*T*-4; *T*+4]. Ramp events are divided into two categories: ramp-up events (increase in wind speed within 4 hours) and ramp-down events (decrease in wind speed within 4 hours) (Freedman *et al*. 2008). Both the observed and forecasted ramps are determined using the 10-min data.

First, we examine the overall performance of the Kalman filter bias correction for improving the forecast skill of ramp events. From Table 4, we know that for the observed 723 ramp events, there are 360 ramp-up events and 363 ramp-down events. The bias correction overestimates the total events both for up-ramps and down-ramps, and does not improve this metric compared with direct model output. But for metrics based on hits, false alarms, misses, and correct nulls, the Kalman filter shows noticeable improvements (see Fig. 9 and Table 4). For the ramp-up events, it shows that of the 360 events, only 98 are correct, indicating that 262 ramp events are missed by the model. The bias correction increases the hits from 98 to 142, and decreases the misses from 262 to 218. And meanwhile, it decreases the false alarms from 292 to 262, and increases the correct nulls from 1628 to 1658. Similarly, for the ramp-down events, the Kalman filter increases the hits and correct nulls from 94 to 139 and from 1662 to 1671 respectively, and decreases the misses and false alarms from 269 to 224 and from 255 to 246 respectively.

To further assess the ability of the Kalman filter bias correction, POD, FAR, TS and TSS scores are calculated (Table 4). The values of POD, FAR, TS and TSS range from 0 to 1 with perfect forecasts having the POD, TS and TSS scores near 1, and an FAR score near zero. The most important statistics are POD and TSS scores, which researchers refer to as the hit rate more commonly (Jolliffe and Stephenson 2012). Table 4 indicates that up-ramps have slightly higher POD score, suggesting that the model predicts up-ramps more accurately compared with down-ramps. The bias correction increases the POD score from 0.27 to 0.39, detecting ramp-up events nearly 40% of the time. After bias correction, the TSS score is significantly

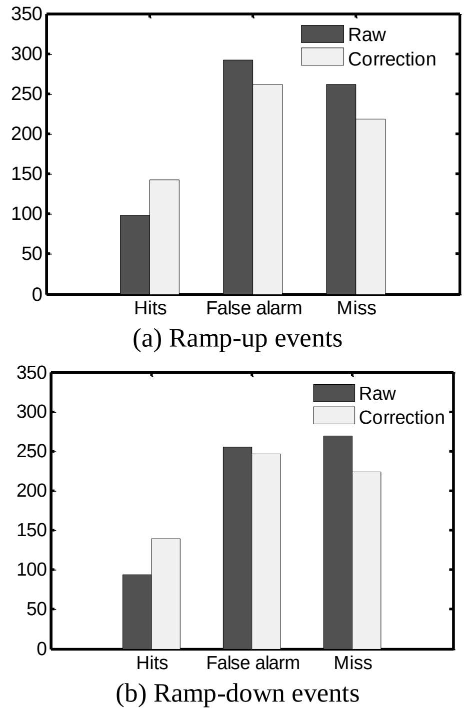

(a) Ramp-up events

(b) Ramp-down events

Fig. 9 Hits, false alarms, and misses of the raw forecasts and the bias correction for ramp events

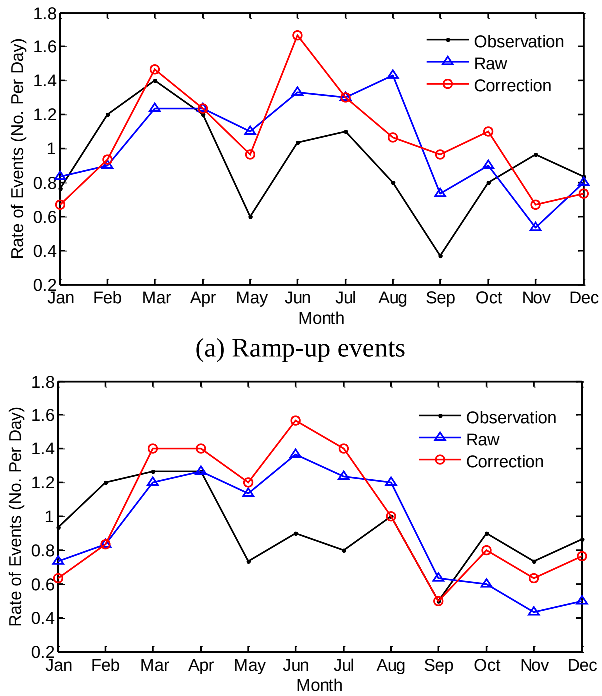

(a) Ramp-up events

(b) Ramp-down events

Fig. 10 Monthly climatology of the observation, the raw forecasts and the bias correction for ramp events per day over a 4-h window

promoted from 0.12 to 0.26 for up-ramps and from 0.13 to 0.25 for down-ramps.

We investigated the basic climatology of the ramp events after bias correction in more detail in Fig. 10. A strong bimodal peak cycle exists with maxima in March and

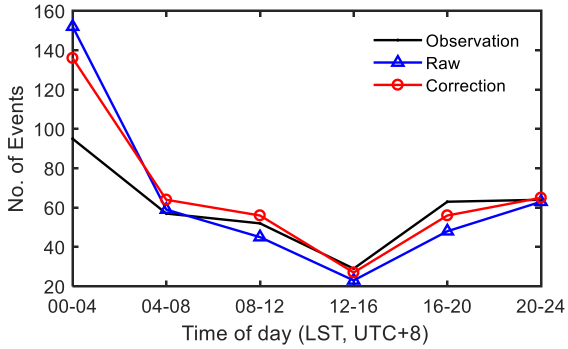

(a) Ramp-up events

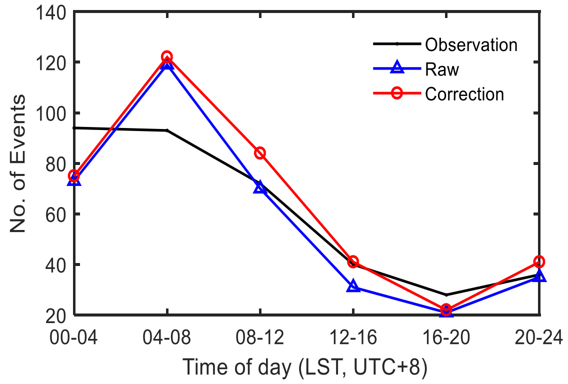

(b) Ramp-down events

Fig. 11 Diurnal variation of the observation, the raw forecasts and the bias correction for ramp events (total number over a 2-yr period centered within 4-h bins) using 4-h definition of ramps

July and decreases between the two peaks with minima in May and September for observed ramp-up events. Results are similar for observed ramp-down events. Observed up-ramps show on average the maximum frequency of 1.4 day^{-1} during March and the minimum of 0.37 day^{-1} during September. For down-ramps the maximum frequency is 1.27 day^{-1} during March-April and the minimum is 0.5 day^{-1} during September. The model and the bias correction both exhibit the basic climatology pattern, and overestimate the rate of events in most of the months for up-ramps and down-ramps. However, the Kalman filter improves the results in March, May, August, and November for up-ramps, and the results in August, September, October, November and December for ramp-down events.

Furthermore, we examined the diurnal variation of the ramp events (Fig. 11). We found that observed up-ramps mostly happen during 00-04 LST, which perhaps is associated with the formation of the low level jet. Observed ramp-down events are most common during 00-08 LST, almost the whole nighttime. In the daytime, both up-ramps (12-16 LST) and down-ramps (16-20 LST) seldom occur. The model exhibits general diurnal trend for the up-ramps, while during 00-04 LST it overestimates the number of events dramatically. The Kalman filter improves the forecast skill for up-ramps during almost all hours, especially reducing the number from 152 to 136 during 00-04 LST. For ramp-down events, the Kalman filter improves the forecast skill moderately during most of the hours.

6. Conclusions

The postprocessing method of nonlinear Kalman filter was proposed to better simulate nonlinear problems in numerical weather prediction. To deal with the high nonlinearity of real-time wind speed forecasts and to improve the wind ramp event forecasts, the nonlinear Kalman filter bias correction method was applied to 24-h wind speed forecasts at 70-m height issued from the WRF model. And the bias correction was tested with observations from Zhangbei wind farm, Hebei Province, China for a two-year period. Conclusions can be summarized as follows.

Sensitivity tests of the nonlinear Kalman filter to polynomial order and time delay were conducted to obtain the optimal filter based on the best forecast performance. The results show a second order polynomial Kalman filter with one-hour time delay is the optimal one. The bias correction has decreased RMSE by 32% from 3.26 m s^{-1} to 2.21 m s^{-1}, decreased MAE by 34% from 2.52 m s^{-1} to 1.66 m s^{-1}, reduced BIAS almost to zero, and improved correlation from 0.58 to 0.82. Moreover, the bias correction improves the forecast skill in almost all wind speed intervals, especially in intervals sensitive to wind power prediction. The fact shows that the Kalman filter is especially suitable for wind power prediction. In addition, the bias correction is able to produce skillful correction upon the raw forecasts, even under abrupt weather transition conditions and in time of the day when the model exhibits large errors. It demonstrates the robustness of the method.

As to the overall performance of the bias correction for ramp event forecasts, the Kalman filter shows noticeable improvements, increasing the hits and correct nulls and decreasing the misses and false alarms substantially for both the ramp-up and ramp-down events. The bias correction increases the POD score of up-ramps from 0.27 to 0.39, detecting up-ramps nearly 40% of the time. Meanwhile, the POD score of down-ramps is increased from 0.26 to 0.38. And the TSS score increases from 0.12 to 0.26 for up-ramps and from 0.13 to 0.25 for down-ramps. Almost doubled TSS score shows the significant promotion for the bias correction in ramp event forecasts. In addition, the diurnal variation of ramp events shows that observed up-ramps usually arise during the early evening, mostly associated with the low level jet. The Kalman filter improves the forecast skill for up-ramps during almost all hours, especially during the period with large forecast errors.

From above results, we know that the nonlinear Kalman filter gives an approach to estimate the forecast error of the numerical model, so that effective bias correction can be conducted to improve the raw forecasts. Traditionally, the real-time wind speed forecasts are directly acquired by statistical methods such as ARMA model, artificial neural network (ANN), and support vector machine (SVM), but combine numerical model and statistical method is a new efficient way which can both make use of dynamical and statistical information. In the future, we can apply other statistical methods to model and thus predict the forecast error, and such work may be prospective in real-time wind speed forecasts.

Acknowledgments

This research was supported by National Key R&D Program of China (Technology and application of wind power / photovoltaic power prediction for promoting renewable energy consumption, 2018YFB0904200) and eponymous Complement S&T Program of State Grid Corporation of China (SGLNDKOOKJJS1800266).

References

Bradford, K.T., Carpenter, R.L. and Shaw, B. (2010), “Forecasting southern plains wind ramp events using the WRF model at 3-km”, *Proceedings of the 9th Annual Student Conference*, Atlanta, U.S.A, January.

Burton, T., Jenkins, N., Sharpe, D. and Bossanyi, E. (2001), *Wind Energy Handbook*, John Wiley & Sons, Ltd, Chichester, West Sussex, England.

Chen, F. and Dudhia, J. (2001), “Coupling an advanced land-surface/hydrology model with the Penn State/NCAR MM5 modeling system. Part I: Model description and implementation”, *Mon. Wea. Rev.*, **129**(4), 569-585. https://doi.org/10.1175/15200493(2001)129<0569:CAALSH>2.0.CO;2.

Chen T.H. and Tran, V.T. (2015), “Prospects of wind energy on Penghu Island, Taiwan”, *Wind Struct.*, **20**(1), 1-13. https://doi.org/10.12989/was.2015.20.1.001.

Cheng, X.L., Li, J., Hu, F., Xu, J. and Zhu, R. (2015), “Refined numerical simulation in wind resource assessment”, *Wind Struct.*, **20**(1), 59-74. http://dx.doi.org/10.12989/was.2015.20.1.059.

Chou M.D. and Suarez, M.J. (1994), “An efficient thermal infrared radiation parameterization for use in general circulation models”, NASA Tech. Memo., NASA, U.S.A.

Costa, A., Crespo, A., Navarro, J., Lizcano, G., Madsen, H. and Feitosa, E. (2008), “A review on the young history of the wind power short-term prediction”, *Renew. Sustain. Energy Rev.*, **12**(6), 1725-1744. https://doi.org/10.1016/j.rser.2007.01.015.

Crochet, P. (2004), “Adaptive Kalman filtering of 2-m temperature and 10-m wind-speed forecasts in Iceland”, *Meteor. Appl.*, **11**, 173-187.

Delle Monache, L., Nipen, T., Deng, X., Zhou, Y. and Stull, R. (2006), “Ozone ensemble forecasts: 2. A Kalman-filter predictor bias correction”, *J. Geophys. Res.*, **111**, D05308, https://doi.org/10.1029/2005JD006311.

Delle Monache, L., Nipen, T., Liu, Y., Roux, G. and Stull, R. (2011), “Kalman filter and analog schemes to post-process numerical weather predictions”, *Mon. Weather. Rev.*, **139**, 3554-3570. https://doi.org/10.1175/2011MWR3653.1.

Monache, L.D., Wilczak, J., McKeen, S., Grell, G., Pagowski, M., Peckham, S., Stull, R., Mchenry, J. and McQueen, J. (2008), “A Kalman-filter bias correction method applied to deterministic, ensemble averaged and probabilistic forecasts of surface ozone”, *Tellus*, **60**(2), 238-249. https://doi.org/10.1111/j.1600-0889.2007.00332.x.

Deppe, A.J., Gallus, W.A. and Takle, E.S. (2013), “A WRF ensemble for improved wind speed forecasts at turbine height”, *Wea. Forecasting*, **28**(1), 212-228. https://doi.org/10.1175/WAF-D-11-00112.1.

Dhunny, A., Lollchund, M. and Rughooputh, S.D.D.V. (2015), “A high-resolution mapping of wind energy potentials for Mauritius using Computational Fluid Dynamics (CFD)”, *Wind Struct.*, **20**(4), 565-578. http://dx.doi.org/10.12989/was.2015.20.4.565.

Francis, N. (2008), *Predicting Sudden Changes in Wind Power Generation*, North American Windpower, October.

Freedman, J., Markus, M. and Penc, R. (2008), “Analysis of west Texas wind plant ramp-up and ramp-down events”, AWS Truewind Report, AWS Truepower, U.S.A.

Galanis, G., Louka, P., Katsafados, P., Pytharoulis, I. and Kallos, G. (2006), “Applications of Kalman filters based on non-linear functions to numerical weather predictions”, *Ann. Geophys.*, **24**, 2451-2460.

Giebel, G. (2001), “On the benefits of distributed generation of wind energy in Europe”, Ph. D. Dissertation, University of Oldenburg, Dusseldorf, Germany.

Glahn, H.R. and Lowry, D.A. (1972), “The use of model output statistics (MOS) in objective weather forecasting”, *J. Appl. Meteor.*, **11**(8), 1203-1211. https://doi.org/10.1175/1520-0450(1972)011<1203:TUOMOS>2.0.CO;2.

Greaves, B., Collins, J., Parkes, J. and Tindal, A. (2009), “Temporal forecast uncertainty for ramp events”, *Wind Eng.*, **33**(4), 309-320.

Gunter, W.S., Schroeder, J.L., Weiss, C.C. and Bruning, E.C. (2017), “Surface measurements of the 5 June 2013 damaging thunderstorm wind event near Pep, Texas”, *Wind Struct.*, **24**(2), 185-204. https://doi.org/10.12989/was.2017.24.2.185.

Hacker, J.P. and Rife, D.L. (2007), “A practical approach to sequential estimation of systematic error on near-surface mesoscale grids”, *Wea. Forecasting*, **22**(6), 1257-1273. https://doi.org/10.1175/2007WAF2006102.1.

Homleid, M. (1995), “Diurnal corrections of short-term surface temperature forecasts using Kalman filter”, *Wea. Forecasting*, **10**(4), 689-707. https://doi.org/10.1175/1520-0434(1995)010<0689:DCOSTS>2.0.CO;2.

Hu, X.M., Klein, P.M. and Xue, M. (2013), “Evaluation of the updated YSU planetary boundary layer scheme within WRF for wind resource and air quality assessments”, *J. Geophys. Res.*, **118**(18), 10490-10505. https://doi.org/10.1002/jgrd.50823.

Janjić, Z.I. (1994), “The step-mountain Eta coordinate model: further developments of the convection, viscous sublayer and turbulence closure schemes”, *Mon. Weather Rev.*, **122**(5), 927-945. https://doi.org/10.1175/15200493(1994)122<0927:TSMECM>2.0.CO;2

Jolliffe, I.T. and Stephenson, D.B. (2012), *Forecast Verification: A Practitioner’s Guide in Atmospheric Science*, (2th Edition), John Wiley & Sons, Ltd, West Sussex, England.

Kain, J.S. (2004), “The Kain-Fritsch convective parameterization: An update”, *J. Appl. Meteor.*, **43**(1), 170-181. https://doi.org/10.1175/15200450(2004)043%3C0170:TKCPAU%3E2.0.CO;2.

Kalman, R.E. (1960), “A new approach to linear filtering and prediction problems”, *J. basic Eng.*, **82**(1), 35-45. https://doi.org/10.1115/1.3662552.

Kalman, R.E. and Bucy, R.S. (1961), “New results in linear filtering and prediction theory”, *J. basic Eng.*, **83**(1), 95-108. https://doi.org/10.1115/1.3658902.

Kalnay, E. (2002), *Atmospheric Modeling, Data Assimilation and Predictability*, Cambridge University Press, Cambridge, Cambridgeshire, U.K.

Lange, M. and Focken, U. (2006), *Physical Approach to Short-term Wind Power Prediction*, Springer, Berlin, Heidelberg, Germany.

Lin, Y.L., Farley, R.D. and Orville, H.D. (1983), “Bulk parameterization of the snow field in a cloud model”, *J. Climate Appl. Meteor.*, **22**(6), 1065-1092. https://doi.org/10.1175/1520-0450(1983)022<1065:BPOTSF>2.0.CO;2.

Louka, P., Galanis, G., Siebert, N., Kariniotakis, G., Katsafados, P., Pytharoulis, I. and Kallos, G. (2008), “Improvements in wind speed forecasts for wind power prediction purposes using Kalman filtering”, *J. Wind Eng. Ind. Aerod.*, **96**(12), 2348-2362. https://doi.org/10.1016/j.jweia.2008.03.013.

McCollor, D. and Stull, R. (2008), "Hydrometeorological accuracy enhancement via post-processing of numerical weather forecasts in complex terrain", *Wea. Forecasting*, **23**(1), 131-144. https://doi.org/10.1175/2007WAF2006107.1.

Mellor, G.L. and Yamada, T. (1982), "Development of a turbulence closure model for geophysical fluid problems", *Rev. Geophys. Space Phys.*, **20**(4), 851-875. https://doi.org/10.1029/RG020i004p00851.

Mlawer, E.J., Taubman, S.J., Brown, P.D., Iacono, M.J. and Clough, S.A. (1997), "Radiative transfer for inhomogeneous atmosphere: RRTM, a validated correlated-k model for the longwave", *J. Geophys. Res.*, **102**(D14), 16663-16682. https://doi.org/10.1029/97JD00237.

Muller, M.D. (2011), "Effects of model resolution and statistical postprocessing on shelter temperature and wind forecasts", *J. Appl. Meteor.*, **50**(8), 1627-1636. https://doi.org/10.1175/2011JAMC2615.1.

Powers, J.G. (2007), "Numerical prediction of an Antarctic severe wind event with the Weather Research and Forecasting (WRF) Model", *Mon. Weather. Rev.*, **135**(9), 3134-3157. https://doi.org/10.1175/MWR3459.1.

Rife, D.L. and Davis, C.A. (2005), "Verification of temporal variations in mesoscale numerical wind forecasts", *Mon. Wea. Rev.*, **133**(11), 3368-3381. https://doi.org/10.1175/MWR3052.1.

Rincon, A., Jorba, O. and Baldasano, J.M. (2010), "Development of a short-term irradiance prediction system using post-processing tools on WRF-ARW meteorological forecasts in Spain", *10th EMS Annual Meeting*, Zurich, Switzerland, September.

Skamarock, W.C., Klemp, J.B., Dudhia, J., Gill, D.O., Barker, D. M., Duda, M.G., Huang, X., Wang, W. and Powers, J.G. (2008), "A description of the Advanced Research WRF version 3", NCAR Technical Note, NCAR, U.S.A.

Stensrud, D.J. and Yussouf, N. (2003), "Short-range ensemble predictions of 2-m temperature and dewpoint temperature over New England", *Mon. Weather Rev.*, **131**(10), 2510-2524. https://doi.org/10.1175/15200493(2003)131%3C2510:SEPOMT%3E2.0.CO;2.

Xu, J.J., Hu, F., Xiao, Z.N. and Li, J. (2013), "Analog bias correction of numerical model on wind power prediction", *J. Appl. Meteorol. Sci.* (In Chinese), **24**(6), 731-740.

Xu, J.J., Hu, F., Xiao, Z.N. and Cheng, X.L. (2014), "Bias correction to wind direction forecast by the circular - circular regression method", *Atmos. Oceanic Sci. Lett.*, **7**, 87-91.

Yang, Q., Berg, L.K., Pekour, M., Fast, J.D., Newsom, R.K., Stoelinga, M. and Finley, C. (2013), "Evaluation of WRF-predicted near-hub-height winds and ramp events over a Pacific Northwest site with complex terrain", *J. Appl. Meteor. Climatol.*, **52**(8), 1753-1763. https://doi.org/10.1175/JAMC-D-12-0267.1

Yim, S.H., Fung, J.C., Lau, A.K. and Kot, S.C. (2007), "Developing a high-resolution wind map for a complex terrain with a coupled MM5 CALMET system", *J. Geophys. Res.*, **112**(D5), https://doi.org/10.1029/2006JD007752.

Zack, J.W. (2007), "Optimization of wind power production forecast performance during critical periods for grid management", *In Proceedings of the European Wind Energy Conference EWEC*, Milano. Italy.

Zhang, H., Pu, Z. and Zhang, X. (2013), "Examination of errors in near-surface temperature and wind from WRF numerical simulations in regions of complex terrain", *Wea. Forecasting*, **28**(3), 893-914. https://doi.org/10.1175/WAF-D-12-00109.1.

FR